Article ID: 1006-8775(2026)03-0229-10

The Rapid Shrinkage in Tropical Cyclone Sizes over the Western North Pacific

YUAN Jin-nan (袁金南), WEN Guan-huan (温冠环), ZHOU Ming-sen (周明森), ZHU Yu (朱 宇), ZHU Yong (朱 泳)
(Guangzhou Institute of Tropical and Marine Meteorology of China Meteorological Administration, Guangdong-Hong Kong-Macao Greater Bay Area Academy of Meteorological Research, Guangzhou 510640 China)

Abstract: This study is the first to comprehensively investigate the climatology and environmental conditions of rapid shrinkage (RS) in four tropical cyclone (TC) sizes, including radii of the outermost closed isobar (ROCI), 17.5 m s^{-1} winds (R17), 25.7 m s^{-1} winds (R26), and 32.9 m s^{-1} winds (R33) over the western North Pacific (WNP) during 2004–2022. The 5th percentile of the 24-h change rate of TC size was used to define the RS in TC size, and the range between the 5th and 95th percentiles of the 24-h change rate of TC size was used to define the non-rapid change (non-RC) in TC size. The RS thresholds for the four TC sizes over the WNP were then obtained. The initial mean sizes and initial mean latitudes of the TC centers of the RS cases were larger and higher than those of the non-RC cases. RS in TC sizes mainly occurred during the decay stage, except for RS in ROCI. Composite analysis showed that environmental conditions such as sea surface temperature, temperature profile, relative humidity profile, and inward angular momentum transport of the RS cases were favorable for RS in TC size. The mean brightness temperature and mean hourly rainfall rate of RS and non-RC in R17, R26, and R33 showed that they were in a significantly more unfavorable convective environment for RS than for non-RC. The environmental conditions differed among the RS of the four TC sizes. Sea surface temperature and atmospheric conditions may cause RS in TC sizes mainly by influencing atmospheric instability, atmospheric moisture, TC precipitation, vertical motion of the TC, radial inflow, and tangential wind of the TC.

Key words: tropical cyclone sizes; rapid shrinkage; tropical cyclone factors; environmental conditions; composite analysis

CLC number: P444 **Document code:** A

Citation: Yuan, J. N., G. H. Wen, M. S. Zhou, Y. Zhu, and Y. Zhu, 2026: The Rapid Shrinkage in Tropical Cyclone Sizes over the Western North Pacific. *J. Trop. Meteor.*, **32**, 229–238, https://doi.org/10.3724/j.1006-8775.2026.002.

1 INTRODUCTION

Tropical cyclone (TC) size usually refers to a parameter represented by radius of outermost closed isobar (ROCI), gale-force winds (17.5 m s^{-1}, R17), damaging-force winds (25.7 m s^{-1}, R26), or hurricane-force winds (32.9 m s^{-1}, R33) (Brand 1972; Kimball and Mulekar 2004; Merrill 1984; Wu and Lei 2014; Yuan et al. 2007; Zhang and Chan 2023). TC size is often associated with potential impacts (Holland and Merrill 1984; Houston et al. 1999; Irish et al. 2008; Powell and Reinhold 2007), areal coverage, and rainfall distributions of TCs (Kidder et al. 2005; Lin et al. 2015; Matyas 2010). TC size significantly affects destructive potential as it is often related to the areal coverage of a storm's precipitation field, which in turn modulates the extent of the inland flooding risk (Weatherford and Gray 1988). Storm surges are also a function of TC size, with larger TCs systematically generating more pronounced surges. Irish et al. (2008) suggested that surges can vary by as much as 30% with realistic changes in TC size. From a socioeconomic viewpoint, larger TCs typically require more extensive evacuation coverage and longer lead times than smaller storms of an equivalent intensity (Whitehead 2003). Therefore, larger TCs tend to be more damaging and expensive (Quiring et al. 2011).

Researchers have identified multiple factors that influence TC size, including both external forcings and internal processes (Chen and Liu 1997; Liu and Chan 2002; MacLay et al. 2008; Weatherford and Gray 1988). One of the internal processes, known as the eyewall replacement cycle, is characterized by the formation of a secondary outer eyewall that contracts radially until it replaces the existing smaller inner eyewall, ultimately resulting in the expansion of the surface wind field (Willoughby et al. 1982). The expansion of the surface wind field can pose heightened risks during landfall because of the increased extent of coastal exposure to storm surge inundation and wind damage. TC size is intrinsically linked to large-scale environmental conditions and other properties that have previously been identified as key determinants of TC size variability (Chan and Yip 2003; Song et al. 2020; Weatherford and Gray 1988). A study of typhoons in the western North Pacific (WNP)

Received 2025-03-24; **Revised** 2025-10-16; **Accepted** 2025-11-21

Funding: National Natural Science Foundation of China (42275123); Guangdong Basic and Applied Basic Research Foundation (2022A1515011100, 2024A1515010508); Guangdong Provincial Marine Meteorology Science Data Center (2024B1212070014); Science and Technology Research Projects of Guangdong Meteorological Service (GRMC2022M02); Innovation Team of Severe Weather Mechanism and Forecasting Technology in the South China Sea of the Guangdong Provincial Meteorological Bureau (GRMCTD202201)

Biography: YUAN Jin-nan, Ph. D., primarily undertaking research on tropical cyclones.

Corresponding author: WEN Guan-huan, e-mail: ghwen@gd121.cn

found that the interannual variability in their mean size could be related to annual variations in synoptic-scale flow patterns (Chan and Yip 2003). Internal dynamics and synoptic-scale forcings have been suggested as key factors determining TC size (Cocks and Gray 2002). Seasonal subtropical ridge activity has also been identified as a potential factor affecting TC size (Chan and Chan 2012). Variations in the lower-tropospheric angular momentum transport and synoptic-scale flow in the vicinity of the TC play a critical role in modulating changes in TC size (Chan and Chan 2013). However, Knaff et al. (2014) suggested that changes in TC size exhibited no explicit latitudinal dependence. Chen et al. (2021) found that the rate of change in TC size over the WNP is significantly correlated with both TC size and intensity.

Rapid changes (RCs) in TC sizes are important for disaster prevention and mitigation. The rapid shrinkage (RS) of the TC size indicates that the disaster range caused by TC is rapidly decreasing. Accurate forecasting of the RS of a TC can avoid excessive defense in disaster prevention. Li et al. (2022, 2023) investigated the rapid growth (RG) of the gale-force wind radius in the WNP by defining it as the 90th percentile of its 24-h change. However, the RS of the TC sizes in WNP has not yet been sufficiently studied.

The primary objectives of this study were to comprehensively investigate the RS of four TC sizes (ROCI, R17, R26, and R33) over the WNP and to examine their associated environmental conditions.

2 DATA AND METHODS

2.1 *Data*

The 6-h best track data of TCs over the WNP during 2004–2022 were obtained from the Joint Typhoon Warning Center (JTWC) via the International Best Track Archive for Climate Stewardship. These data, which consist of the 6-hourly estimates of position, maximum sustained wind speed (v_{max}), minimum central pressure, size parameters, and other relevant variables (Knapp et al. 2010), are publicly accessible at https://www.ncei.noaa.gov/products/international-best-track-archive. The size parameters comprise ROCI, radii of 34 knot (17.5 m s^{-1}) winds in each quadrant (R17), radii of 50 knot (25.7 m s^{-1}) winds in each quadrant (R26), radii of 64 knot (32.9 m s^{-1}) winds in each quadrant (R33), radii of maximum winds, and the eye diameter.

Daily sea surface temperature (SST) data, derived from the microwave and infrared (MW-IR) optimal interpolation product with a spatial resolution of 9 km, were produced by Remote Sensing Systems. This dataset was sponsored by the National Oceanographic Partnership Program and the National Aeronautics and Space Administration Earth Science Physical Oceanography Program, and is available at http://www.remss.com. High-resolution daily SST data from the MW-IR have high horizontal resolution and small bias in the coastal waters of the WNP (Yuan et al. 2016). Atmospheric data were derived from the National Centers for Environmental Prediction (NCEP) Final Operational Global Analysis data, which are available at the surface and 26 standard pressure levels (from 1000 to 10 hPa) on 1-degree by 1-degree latitude-longitude grids at 6-hourly intervals (National Centers for Environmental Prediction et al. 2000) and are available at https://rda.ucar.edu/datasets/d083002/.

Hourly IR brightness temperature data with a resolution of 0.25°×0.25° were derived from the Japanese Geostationary Meteorological Satellite/Multifunctional Transport Satellites (GMS/MTSAT) and are available at http://weather.is.kochi-u.ac.jp/sat/ALL/.

The hourly rainfall rate data were obtained from the Tropical Rainfall Measuring Mission (TRMM) 3B42 dataset, which is at 3-hourly and 0.25°×0.25° latitude-longitude resolutions (Huffman et al. 2007), and are available at https://disc.gsfc.nasa.gov/TRMM. Hourly rainfall rate data existed only before 2019, and only data from 2004 to 2019 were used in this study.

2.2 *Methods*

The JTWC has recorded radii of 35-kt winds in four quadrants from 2001 onward. Beginning in 2004, the JTWC additionally included 50-kt and 64-kt wind radii, replacing 35-kt with 34-kt (Song and Klotzbach 2016). Therefore, four TC sizes (ROCI, R17, R26, and R33) from 2004 to 2022 were analyzed in this study. Additionally, there may be some uncertainty in the TC size data estimated from the JTWC best tracks, which is not discussed in this study. R17, R26, and R33 use mean values of the four quadrants. For quality control purposes, samples of R17, R26, and R33 were not considered, as some quadrants had missing values. Samples north of 40°N were not considered to filter out the effect of the extratropical transition on TC size change (Hart and Evans 2001).

To systematically examine common features, only events with RS in TC sizes in which the TC circulation (the area from the TC center to ROCI) remained entirely over the open ocean of the WNP during 2004–2022 were considered. RS events that occurred when TC circulation interacted with marginal seas or land were deliberately excluded to minimize coastal interference effects. To objectively determine whether TC circulation remained entirely over the ocean during RS in terms of TC size, high-resolution bathymetry data derived from the ETOPO5 dataset were employed. Specifically, a grid-based criterion was applied: if the bathymetric depth at all grid points within the TC circulation domain in the WNP was below zero (i.e., <0 m), the TC circulation was classified as entirely over the ocean.

Similar to the methodology applied to define rapid weakening in TC intensity (Ma Z H et al. 2019), the present study adopted the 5th percentile of the 24-h change rate of TC size as a threshold for RS (Fig. 1). Conversely, the non-rapid change (non-RC) was defined using the range between the 5th and 95th percentiles of the 24-h

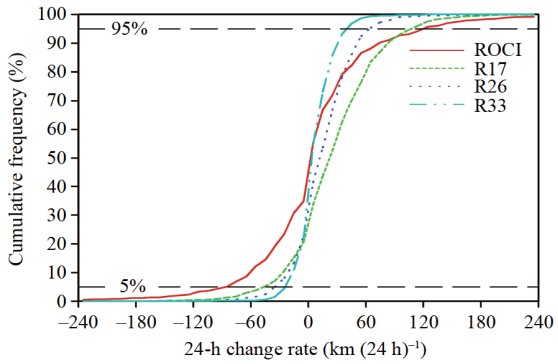


Figure 1. Cumulative frequency distribution of over-water 24-h change rates of four TC sizes over the WNP during 2004–2022.

change rate of TC size, while RG was characterized by values reaching the 95th percentile of this change rate. If the 10th percentile proposed by Li et al. (2023) is used to define the RS in terms of TC size, the results will not be significantly different and only the differences in the TC variables and environmental conditions between the RS and non-RC cases will be less pronounced. The 24-h change in TC size ($dR_{24\,h}$) was calculated for each discrete 24-h interval by subtracting the initial TC size at time t=0 h ($R_{0\,h}$) from the final TC size at time t=24 h ($R_{24\,h}$), expressed as $dR_{24\,h} = R_{24\,h} - R_{0\,h}$. The dataset of 24-h change in TC size comprises all overlapping 24-h periods for every TC.

The absolute angular momentum flux (AAMF) across a circle centered at the TC center at radius is given by (Chan and Chan 2013)

$$\mathrm{AAMF}(r) = \int_0^{2\pi}\left(v_\theta r + \frac{1}{2}fr^2\right)v_r r\,\mathrm{d}\theta \Big/ \int_0^{2\pi} r\,\mathrm{d}\theta \qquad (1)$$

where r is the radius from the TC center, v_θ is the tangential wind, f is the Coriolis parameter, v_r is the radial wind, and θ is the azimuth.

The statistical significance of the difference between the means of RS and non-RC cases was assessed based on the non-parametric bootstrap method (Efron 1979).

3 RS IN TC SIZES OVER THE WNP DURING 2004–2022

The over-water 24-h change rates of ROCI, R17, R26, and R33 over the WNP during 2004–2022 were calculated from 233 TCs, with 2897, 2897, 1905, and 1285 samples, respectively (Table 1). The RS events of the four TC-size categories had different sample sizes: 145 cases for ROCI, 145 for R17, 95 for R26, and 64 for R33. The corresponding 5th percentiles of over-water 24-h change rates (km (24 h)$^{-1}$) were −83.3 (ROCI), −41.7 (R17), −30.1 (R26), and −18.6 (R33), respectively, establishing the thresholds for RS classification within each of the four TC size categories over the WNP (Table 1 and Fig. 1).

The initial mean sizes of the RS cases were larger than those of the non-RC cases, and all were statistically significant at 95% confidence level (Table 2). The initial

Table 1. The 5th percentiles of over-water 24-h change rates of four TC sizes over the WNP during 2004–2022.

TC size	Total samples	RS samples	5th percentile of 24-h change rate (km (24 h)$^{-1}$)
ROCI	2897	145	−83.3
R17	2897	145	−41.7
R26	1905	95	−30.1
R33	1285	64	−18.6

Table 2. Initial (at t = 0 h) mean values of TC variables of the RS and non-RC cases for the four TC sizes. TC LAT indicates the latitude of the TC center. The superscript "*" indicates that the difference between RS and non-RC is statistically significant at 95% confidence level, from the results of a non-parametric bootstrap method.

TC variable	RS	non-RC
Initial mean ROCI (km)	488.3*	378.4
Initial mean R17 (km)	259.9*	193.8
Initial mean R26 (km)	163.2*	108.5
Initial mean R33 (km)	90.4*	66.7
Initial mean TC LAT for ROCI	19.6°N	19.0°N
Initial mean TC LAT for R17	21.1°N*	18.9°N
Initial mean TC LAT for R26	20.2°N*	18.8°N
Initial mean TC LAT for R33	19.2°N	18.9°N
Initial mean v_{max} for ROCI (m s^{-1})	37.0	38.8
Initial mean v_{max} for R17 (m s^{-1})	40.3	38.9
Initial mean v_{max} for R26 (m s^{-1})	45.4	46.6
Initial mean v_{max} for R33 (m s^{-1})	57.4*	52.9
24-h change in mean v_{max} for ROCI (m s^{-1})	4.6	4.3
24-h change in mean v_{max} for R17 (m s^{-1})	−4.7	4.7
24-h change in mean v_{max} for R26 (m s^{-1})	−3.5	4.1
24-h change in mean v_{max} for R33 (m s^{-1})	−6.1	2.4

mean latitude of the TC center in the RS cases was higher than that of the non-RC cases, and the RS cases in the R17 and R26 size categories exhibited statistical significance at 95% confidence level (Table 2). The initial mean maximum wind speed v_{max} of the RS cases was higher in the R17 and R33 sizes than in the non-RC cases, whereas the RS cases of ROCI and R26 showed lower v_{max} values relative to their respective non-RC cases (Table 2). The 24-h changes in mean v_{max} of RS and non-RC in ROCI were 4.6 and 4.3 m s^{-1}, respectively, indicating that both RS and non-RC in ROCI events predominantly occurred during the intensification stage. In contrast, the 24-h changes in the mean v_{max} of RS (non-RC) in R17, R26, and R33 were negative (positive) (Table 2), demonstrating that RS (non-RC) in R17, R26, and R33 occurred primarily during the decay (intensification) stage. The percentages of weakened TC intensity in the RS cases of ROCI, R17, R26, and R33 were 26.2%, 62.1%, 62.1%, and 70.3%, respectively (Table 3). However, the percentages of rapid weakening of TC intensity in the RS cases of ROCI, R17, R26, and R33 were 2.1%, 15.2%, 10.5%, and 23.4%, respectively. Therefore, the RS of the TC size was not significantly

Table 3. Percentages of weakening and rapid weakening of TC intensity in RS cases for the four TC sizes. The 5th percentile of the 24-h change in v_{max} in 2897 samples was used to define the rapid weakening of TC intensity.

Change in TC size	Percentage of weakening of TC intensity (%)	Percentage of rapid weakening of TC intensity (%)
RS in ROCI	26.2	2.1
RS in R17	62.1	15.2
RS in R26	62.1	10.5
RS in R33	70.3	23.4

related to the rapid weakening of the TC intensity (Table 3). The 24-h tracks of the RS cases of ROCI, R17, R26, and R33 over the WNP during 2004–2022 are shown in Fig. 2. The RS cases of ROCI (Fig. 2a) and R17 (Fig. 2b) occurred predominantly in the region between 125°–165°E and 5°–40°N. The RS cases of R26 (Fig. 2c) and R33 (Fig. 2d) were primarily concentrated between 130°–155°E and 10°–35°N.

The RS cases occurred mainly during the typhoon season, from July to November, exhibiting temporal distribution patterns consistent with those of the non-RC cases (not shown). The statistical results showed that the RS cases of ROCI and R17 predominantly preceded a TC's peak intensity, whereas the RS cases of R33 frequently occurred after the TC reached its maximum intensity (Table 4).

4 ENVIRONMENTAL CONDITIONS ASSOCIATED WITH RS IN TC SIZES OVER THE WNP

4.1 *Oceanic conditions*

SST is a critical environmental factor that influences

Table 4. Percentages of RS cases that occurred before and after the strongest TC intensity.

Change in TC size	Percentage that the cases occur before the strongest intensity of a TC (%)	Percentage that the cases occur after the strongest intensity of a TC (%)
RS in ROCI	77.9	20.0
RS in R17	54.5	37.2
RS in R26	46.3	46.3
RS in R33	42.2	45.3

TC size (Lin et al. 2015). Modeling studies have suggested that warmer SSTs favor expansion of TC size by enhancing unstable atmospheric conditions (Ma C et al. 2019; Sun et al. 2017). To characterize the overall oceanic conditions associated with the RS cases, the 24-h SST fields for all RS cases were composited. Fig. 3 shows the composite SST during the 24-h period for the RS cases, along with the difference between the RS and non-RC composite SSTs. Notable differences in the horizontal distribution of composite SST emerged across the RS cases for the four TC sizes (Fig. 3). The composite SST of RS in ROCI near TC center was between 27.5 and 28.0 °C, marginally colder than that of non-RC by approximately 0.1–0.5 °C (Fig. 3a). In contrast, the composite SST of RS in R17, R26, and R33 near the TC center was between 27.0 and 27.5 °C, exhibiting significantly lower temperatures than those of non-RC by about 0.5–1.0 °C at 95% confidence level (Figs. 3b–3d). Fig. 4 displays the box-and-whisker plots of the mean SST within the TC circulation of the RS and non-RC cases during the 24-h period. The mean SST of the RS cases within the TC circulation was lower than that of the non-RC cases,

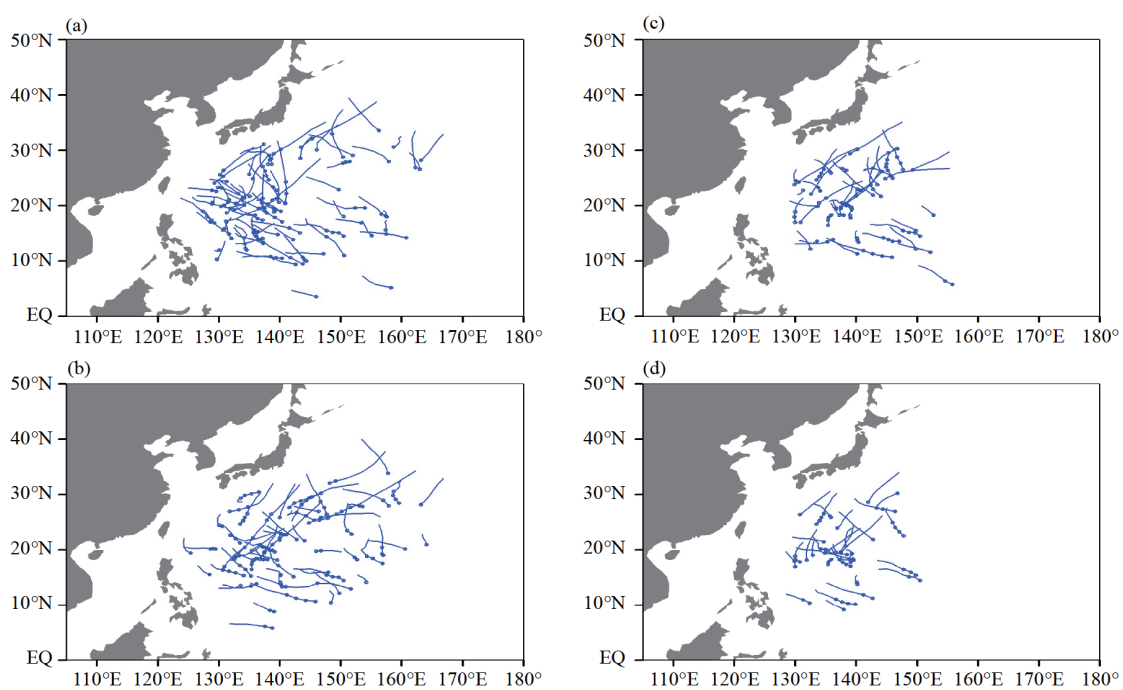


Figure 2. 24-h tracks of RS cases over the WNP during 2004–2022. (a) ROCI, (b) R17, (c) R26, and (d) R33. The dots represent the initial positions (at t = 0 h) of the RS cases.

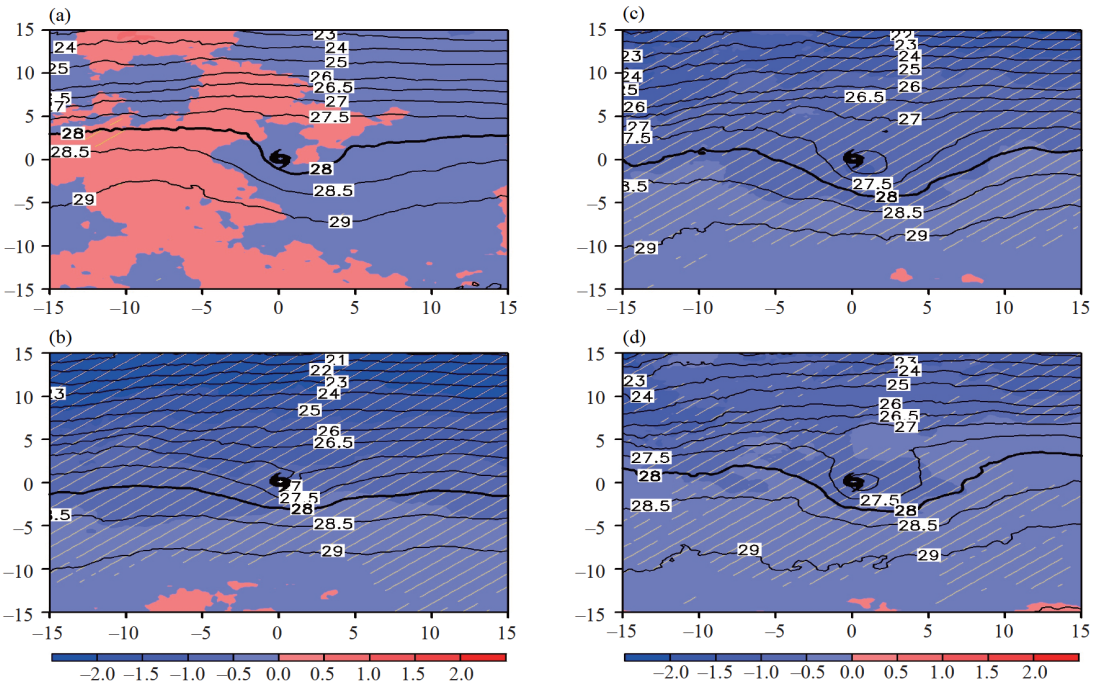


Figure 3. Composite SST (contour, units: °C) of the RS cases and difference of the composite SST (shaded, units: °C) between the RS cases and the non-RC cases during the 24-h period. (a) ROCI, (b) R17, (c) R26, and (d) R33. The bold solid line represents 28.0 °C. The oblique yellow lines indicate that the difference between the RS and non-RC cases is significant at 95% confidence level based on the non-parametric bootstrap method. The typhoon symbol represents the location of the TC center. The *x*-axis and *y*-axis are longitude and latitude relative to the TC center, respectively.

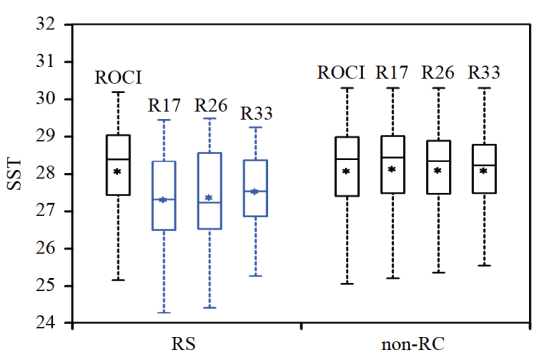


Figure 4. The box-and-whisker plots of the mean SST (units: °C) of the RS cases and the non-RC cases within the TC circulation (defined as the 0–ROCI radius region of TC) during the 24-h period. The box-and-whisker plot diagram was plotted using the numbers of the smallest value, lower quartile (Q1), median, upper quartile (Q3), and largest values. The box shows the quartiles Q1 and Q3, the line in the box marks the median, and the asterisk represents the mean. The blue color indicates that the mean is statistically smaller than that of the non-RC group at 95% confidence level.

except that the RS in ROCI was statistically insignificant at 95% confidence level (Fig. 4). The colder SST of the RS cases may be related to the fact that RS cases usually occur at higher latitudes (Table 2). Colder SST in RS cases may negatively impact key atmospheric processes, including atmospheric instability, atmospheric moisture, TC precipitation, vertical motion, and radial inflow of TC, which may ultimately contribute to RS in terms of TC size (Wang 2009; Yuan et al. 2024).

4.2 *Atmospheric conditions*

Previous simulation results have revealed the critical role of environmental relative humidity (RH) and heating within the outer spiral rainbands in modulating TC size (Hill and Lackmann 2009; Wang 2009; Ying and Zhang 2012). Fig. 5 presents the mean vertical profiles of the difference in temperature and RH between the RS and non-RC cases within the TC surroundings (defined as the ROCI–3ROCI radius region) during the 24-h period. The mean environmental temperature of the RS cases within the TC surroundings below 600 hPa was generally lower than that of the non-RC cases (Fig. 5a), which may be related to lower SST and higher latitudes where RS cases typically occurred (Fig. 4 and Table 2). Below 600 hPa, the difference in temperature between the RS and non-RC cases increased with height, exhibiting statistical significance at 95% confidence level, except for RS in the ROCI category (Fig. 5a). This indicates that the RS cases are generally associated with greater static stability than the non-RC cases in the lower atmosphere. Additionally, the difference in temperature between the RS and non-RC was most pronounced for R17 and least pronounced for ROCI below 600 hPa. The mean environmental RH of the RS in the ROCI within the TC surroundings from 650 to 200 hPa was lower than that of the non-RC (Fig. 5b). Similarly, the mean environmental RH of the RS in R17, R26, and R33 within the TC surroundings from 850 to 200 hPa exhibited significantly drier conditions (lower RH) than that of non-RC at 95% confidence level (Fig. 5b). The difference in RH between

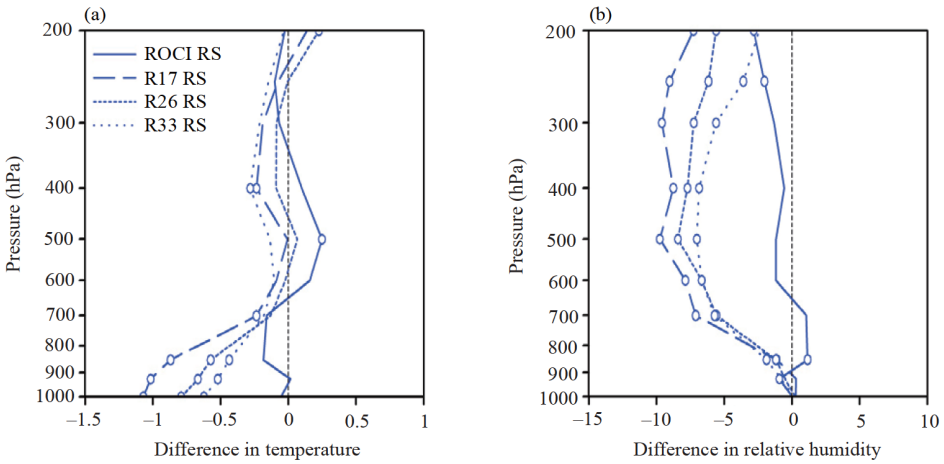


Figure 5. Mean vertical profiles of the difference in (a) temperature (units: K) and (b) relative humidity (units: %) between the RS cases and the non-RC cases within the TC surroundings (defined as the ROCI–3ROCI radius region of the TC) during the 24-h period. The open circles indicate that the difference between the RS and non-RC groups was significant at 95% confidence level.

the RS and non-RC cases was most pronounced for R17 and least pronounced for ROCI within this layer. The colder environmental temperatures in the RS cases may suppress atmospheric instability and TC precipitation, whereas the drier environmental conditions (lower RH) in the RS cases may further limit atmospheric moisture availability and TC precipitation processes, both of which likely contribute to the RS in TC sizes.

Figure 6 shows the composite brightness temperature of the RS cases and the difference in the composite brightness temperature between the RS and non-RC cases during the 24-h period. The composite brightness temperature on the southern side of the TC circulation was higher for the RS cases than for the non-RC cases, with statistically significant differences (at 95% confidence level) observed for R17 and R26. The mean brightness temperature of the RS cases of R17, R26, and R33 within the TC surroundings during the 24-h period was significantly higher than that of non-RC at 95% confidence level (Table 5). In contrast, the RS cases of ROCI within the TC surroundings indicated a slightly colder mean brightness temperature than the non-RC cases during the 24-h period (Table 5). Meanwhile, the mean hourly rainfall rate of the RS cases of R17, R26, and R33 within the TC surroundings was lower than that of the non-RC cases, whereas the RS in ROCI displayed a slightly

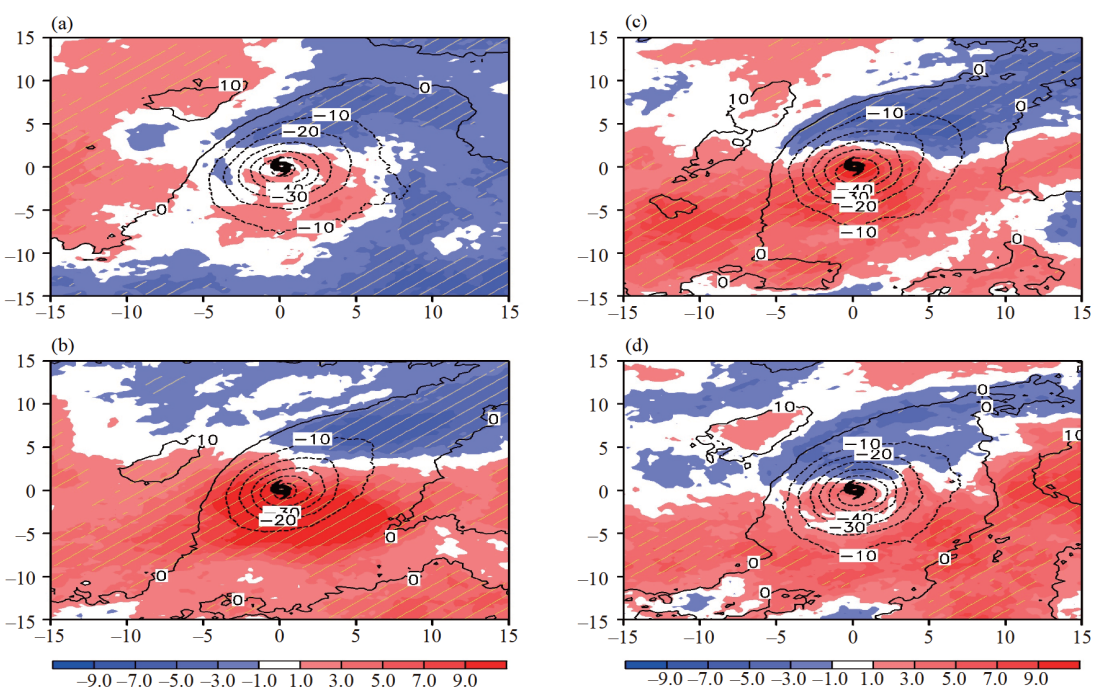


Figure 6. Composite brightness temperature (contour, units: °C) of the RS cases and difference of the composite brightness temperature (shaded, units: °C) between the RS cases and the non-RC cases during the 24-h period. (a) ROCI, (b) R17, (c) R26, and (d) R33. The oblique yellow lines indicate that the difference between RS and non-RC cases was significant at 95% confidence level. The typhoon symbol represents the location of the TC center. The *x*-axis and *y*-axis are longitude and latitude relative to the TC center, respectively.

Table 5. Mean brightness temperature of the RS and non-RC cases within the TC surroundings (defined as the ROCI–3ROCI radius region of the TC) during the 24-h period. The superscript "*" indicates that the difference between RS and non-RC is statistically significant at 95% confidence level.

Variable	RS	non-RC
Mean brightness temperature for ROCI (°C)	−5.39	−5.11
Mean brightness temperature for R17 (°C)	−1.38*	−5.19
Mean brightness temperature for R26 (°C)	−1.72*	−5.08
Mean brightness temperature for R33 (°C)	−2.02*	−4.41

higher mean rainfall rate within the TC surroundings during the 24-h period (Fig. 7). These results indicate that the RS cases of R17, R26, and R33 occurred in a significantly more unfavorable convective environment, which was characterized by warmer brightness temperatures and reduced rainfall compared to the non-RC cases.

Angular momentum transport in the lower troposphere is a critical factor affecting TC size, with increased inward angular momentum transport favoring TC growth (Chan and Chan 2013; Chen et al. 2022). Fig. 8 shows the radius-height cross-sectional composite of the AAMF of the RS cases, along with the differences in the composite AAMF between the RS and non-RC cases during the 24-h period. The negative AAMF of the RS cases was mainly concentrated below 800 hPa, indicating inward angular momentum transport in this layer. The composite differences in AAMF between the RS and non-RC cases showed predominantly positive values within a radius of 2°–12° latitudes and between 850 and 400 hPa. These differences are statistically significant at 95% confidence level for ROCI, R17, and R26 across several regions within this layer. These predominantly positive AAMF differences between 850 and 400 hPa indicate that the environmental inward angular momentum transport decreased mainly in the RS cases relative to the non-RC cases. The decrease in inward angular momentum transport dynamically favors the RS cases, as it weakens the radial inflow and tangential wind of the TC, which may further result in RS in the TC sizes. Moreover, the

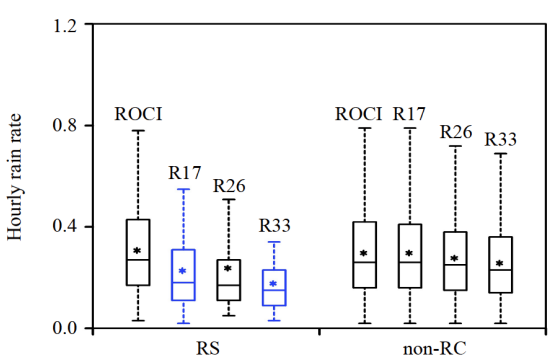


Figure 7. Similar to Fig.4, the mean hourly rainfall rate (units: mm h^{-1}) of the RS and non-RC cases within the TC surroundings (defined as the ROCI–3ROCI radius region of the TC) during the 24-h period.

significant difference in the angular momentum transport between the RS and non-RC cases mainly originates from the axisymmetric component (not shown). Environmental convective features can also affect the environmental angular momentum transport by influencing the tangential and radial winds relative to the TC center. Therefore, there is a dynamic link between the differences in the environmental convective features and those in the environmental angular momentum transport (Figs. 7 and 8).

5 CONCLUSION AND DISCUSSION

In this study, the climatology and environmental conditions associated with RS in four TC sizes (ROCI, R17, R26, and R33) over the open ocean of the WNP during 2004–2022 were comprehensively investigated.

RS in TC size is defined as the 5th percentile of the 24-h change rate of TC size, while non-RC in TC size is defined as the range between the 5th and 95th percentiles of the 24-h change rate of TC size. The thresholds of RS in ROCI, R17, R26, and R33 over the open ocean of the WNP were −83.3, −41.7, −30.1, and −18.6 km $(24\ h)^{-1}$, respectively. Because of the varying background atmospheric and oceanic states (Ma C et al. 2019), the thresholds of RS in TC sizes derived from the WNP conditions may differ in other ocean basins.

The initial mean size and latitude of the TC center were significantly larger and higher for the RS cases than for the non-RC cases, and many of them were statistically significant at 95% confidence level. The R17 and R33 RS cases exhibited a higher initial mean maximum sustained wind (v_{max}) than their non-RC counterparts. RS cases occurred predominantly during the typhoon season from July to November. The RS cases of ROCI and R17 predominantly preceded the TC peak intensity, whereas the RS cases of R33 occurred primarily after the peak intensity. The RS cases for all four TC sizes were most frequent during the TC decay stage, except for ROCI, where this temporal pattern was less pronounced.

The mean SST near the TC center was significantly colder for the RS cases than for the non-RC cases, except that the RS cases of ROCI were statistically insignificant at 95% confidence level. Below 600 hPa, the mean environmental temperature within the TC surroundings was lower and more statically stable in the RS than in the non-RC cases. From 850 to 200 hPa, the mean environmental RH within the TC surroundings during the 24-h period was significantly lower for the RS cases than for the non-RC cases, except for the RS cases of ROCI, in which the difference lacked statistical significance at 95% confidence level. These findings indicate that RS cases are typically associated with cooler, more stable atmospheric conditions and reduced moisture availability, which may contribute to TC size reduction. The exception to ROCI highlights the potential size-specific responses to environmental forcing.

Analyses of the mean brightness temperature and mean hourly rainfall rate within the TC surroundings

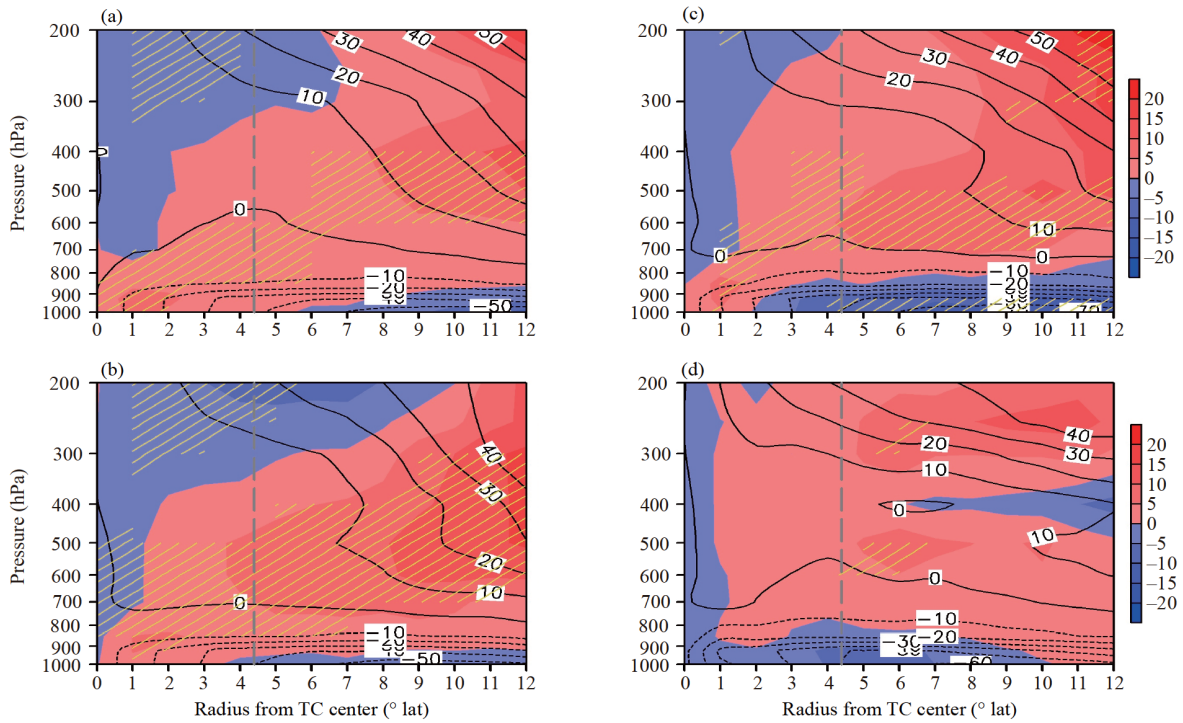


Figure 8. Radius-height cross-sectional composite of AAMF (contour, units: 10^6 m^3 s^{-2}) of the RS cases and differences in the composite AAMF (shaded, units: 10^6 m^3 s^{-2}) between the RS and non-RC cases during the 24-h period. (a) ROCI, (b) R17, (c) R26, and (d) R33. A positive AAMF is indicated outward. The oblique yellow lines indicate that the difference between RS and non-RC cases was significant at 95% confidence level. The thick vertical dashed line indicates the initial (at t = 0 h) mean ROCI of the RS cases.

during the 24-h period revealed that the RS cases of R17, R26, and R33 occurred within a significantly more unfavorable convective environment compared to the non-RC cases. This unfavorable environmental condition was further evidenced by a pronounced decrease in the inward angular momentum transport between 850 and 400 hPa for the RS cases relative to the non-RC cases. Additionally, the environmental conditions differed among the RS of the four TC sizes, suggesting size-specific responses to atmospheric and oceanic forcing.

The SST and atmospheric conditions of the RS cases may contribute to RS in TC size, mainly by modulating atmospheric instability, atmospheric moisture availability, TC precipitation processes, vertical motion within the TC, radial inflow, and tangential wind of the TC. These interacting factors collectively modulate the energy and momentum balance of the TC, thereby driving the shrinkage of its circulation.

ROCI and the other three TC sizes showed noticeably different characteristics. This may be because the ROCI was determined using the outermost closed isobar, whereas the other three TC sizes were determined using wind fields. Additionally, the ROCI describes the outermost range of a TC, whereas the other three TC sizes describe the different internal regions of a TC. The mechanisms affecting the RS in ROCI, R17, R26, and R33 may differ. In operational TC size monitoring, different TC size parameters should be selected according to actual requirements.

Given the limited sample size of RS cases in this study, the conclusions drawn here deserve further validation using expanded datasets in future research. Moreover, the complex interactive effects between the intrinsic TC factors and environmental conditions driving RS across different TC sizes remain insufficiently understood and require further investigation through numerical simulations to systematically investigate these mechanistic relationships and their size-dependent variations.

REFERENCES

Brand, S., 1972: Very large and very small typhoon of the western north Pacific Ocean. *J. Meteor. Soc. Japan*, **50**, 332–341, https://doi.org/10.2151/jmsj1965.50.4_332.

Chan, J. C. L., and C. K. M. Yip, 2003: Interannual variations of tropical cyclone size over the western North Pacific. *Geophys. Res. Lett.*, **30**, 2267, https://doi.org/10.1029/2003GL018522.

Chan, K. T. F., and J. C. L. Chan, 2012: Size and strength of tropical cyclones as inferred from QuikSCAT data. *Mon. Wea. Rev.*, **140**, 811–824, https://doi.org/10.1175/MWR-D-10-05062.1.

Chan, K. T. F, and J. C. L. Chan, 2013: Angular momentum transports and synoptic flow patterns associated with tropical cyclone size change. *Mon. Wea. Rev.*, **141**, 3985–4007, https://doi.org/10.1175/MWR-D-12-00204.1.

Chen, K. X., G. H. Chen, C. H. RAO, and Z. Wang, 2021: Relationship of tropical cyclone size change rate with size and intensity over the western North Pacific. *Atmos. Ocean. Sci. Lett.*, **14**, 100040, https://doi.org/10.1016/j.aosl.2021.100040.

Chen, K. X., G. H. Chen, and D. L. Shi, 2022: Reexamination of the relationship between tropical cyclone size and intensity over the western North Pacific. *Adv. Atmos. Sci.*, **39**, 1956–1968, https://doi.org/10.1007/s00376-022-1450-6.

Chen, L., and S. Liu, 1997: A preliminary analysis on mechanism of size change in tropical cyclone. *J. Trop. Meteor.*, **3**, 122–127.

Cocks, S. B., and W. M. Gray, 2002: Variability of the outer wind profiles of western North Pacific typhoons: Classifications and techniques for analysis and forecasting. *Mon. Wea. Rev.*, **130**, 1989–2005, https://doi.org/10.1175/1520-0493(2002)130<1989:VOTOWP>2.0.CO;2.

Efron, B., 1979: Bootstrap methods: Another look at the jackknife. *Ann. Stat.*, **7**, 1–26, https://doi.org/10.1214/aos/1176344552.

Hart, R. E., and J. L. Evans, 2001: A climatology of the extratropical transition of Atlantic tropical cyclones. *J. Climate*, **14**, 546–564, https://doi.org/10.1175/1520-0442(2001)014<0546:ACOTET>2.0.CO;2.

Hill, K. A., and G. M. Lackmann, 2009: Influence of environmental humidity on tropical cyclone size. *Mon. Wea. Rev.*, **137**, 3294–3315, https://doi.org/10.1175/2009MWR2679.1.

Holland, G. J., and R. T. Merrill, 1984: On the dynamics of tropical cyclone structural changes. *Quart. J. Roy. Meteor. Soc.*, **110**, 723–745, https://doi.org/10.1002/qj.49711046510.

Houston, S. H., W. A. Shaffer, M. D. Powell, and J. Chen, 1999: Comparisons of HRD and SLOSH surface wind fields in hurricanes: Implications for storm surge modeling. *Wea. Forecasting*, **14**, 671–686, https://doi.org/10.1175/1520-0434(1999)014<0671:COHASS>2.0.CO;2.

Huffman, G. J., and Coauthors, 2007: The TRMM multisatellite precipitation analysis (TMPA): Quasi-global, multiyear, combined-sensor precipitation estimates at fine scales. *J. Hydrometeor.*, **8**, 38–55, https://doi.org/10.1175/JHM560.1.

Irish, J. L., D. T. Resio, and J. J. Ratcliff, 2008: The influence of storm size on hurricane surge. *J. Phys. Oceanogr.*, **38**, 2003–2013, https://doi.org/10.1175/2008JPO3727.1.

Kidder, S. Q., J. A. Knaff, S. J. Kusselson, M. Turk, R. R. Ferraro, and R. J. Kuligowski, 2005: The tropical rainfall potential (TRaP) technique. Part I: Description and examples. *Wea. Forecasting*, **20**, 456–464, https://doi.org/10.1175/WAF860.1.

Kimball, S. K., and M. S. Mulekar, 2004: A 15-year climatology of North Atlantic tropical cyclones. Part I: Size parameters. *J. Climate*, **17**, 3555–3575, https://doi.org/10.1175/1520-0442(2004)017<3555:aycona>2.0.co;2.

Knaff, J. A., S. P. Longmore, and D. A. Molenar, 2014: An objective satellite-based tropical cyclone size climatology. *J. Climate*, **27**, 455–476, https://doi.org/10.1175/JCLI-D-13-00096.1.

Knapp, K. R., M. C. Kruk, D. H. Levinson, H. J. Diamond, and C. J. Neumann, 2010: The international best track archive for climate stewardship (IBTrACS): Unifying tropical cyclone data. *Bull. Amer. Meteor. Soc.*, **91**, 363–376, https://doi.org/10.1175/2009BAMS2755.1.

Li, Y., Y. M. Tang, and S. Wang, 2022: Rapid growth of outer size of tropical cyclones: A new perspective on their destructive potential. *Geophys. Res. Lett.*, **49**, e2022GL099230, https://doi.org/10.1029/2022GL099230.

Li, Y., Y. M. Tang, S. Wang, and X. Li, 2023: Rapid growth of tropical cyclone outer size over the western North Pacific. *Remote Sens.*, **15**, 486, https://doi.org/10.3390/rs15020486.

Lin, Y. L., M. Zhao, and M. H. Zhang, 2015: Tropical cyclone rainfall area controlled by relative sea surface temperature. *Nat. Commun.*, **6**, 6591, https://doi.org/10.1038/ncomms7591.

Liu, K. S., and J. C. L. Chan, 2002: Synoptic flow patterns associated with small and large tropical cyclones over the western North Pacific. *Mon. Wea. Rev.*, **130**, 2134–2142, https://doi.org/10.1175/1520-0493(2002)130<2134:SFPAWS>2.0.CO;2.

Ma, C., M. Peng, T. Li, Y. Sun, J. Liu, and M. Bi, 2019: Effects of background state on tropical cyclone size over the western North Pacific and northern Atlantic. *Climate Dyn.*, **52**, 4143–4156, https://doi.org/10.1007/s00382-018-4372-3.

Ma, Z. H., J. F. Fei, and X. G. Huang, 2019: A definition of rapid weakening for tropical cyclones over the western North Pacific. *Geophys. Res. Lett.*, **46**, 11471–11478, https://doi.org/10.1029/2019GL085090.

MacLay, K. S., M. DeMaria, and T. H. Vonder Haar, 2008: Tropical cyclone inner-core kinetic energy evolution. *Mon. Wea. Rev.*, **136**, 4882–4898, https://doi.org/10.1175/2008MWR2268.1.

Matyas, C. J., 2010: Associations between the size of hurricane rain fields at landfall and their surrounding environments. *Meteor. Atmos. Phys.*, **106**, 135–148, https://doi.org/10.1007/s00703-009-0056-1.

Merrill, R. T., 1984: A comparison of large and small tropical cyclones. *Mon. Wea. Rev.*, **112**, 1408–1418, https://doi.org/10.1175/1520-0493(1984)112<1408:acolas>2.0.co;2.

National Centers for Environmental Prediction, National Weather Service, National Oceanic and Atmospheric Administration, and U.S. Department of Commerce, 2000: NCEP FNL operational model global tropospheric analyses, continuing from July 1999. NSF National Center for Atmospheric Research, https://doi.org/10.5065/D6M043C6.

Powell, M. D., and T. A. Reinhold, 2007: Tropical cyclone destructive potential by integrated kinetic energy. *Bull. Amer. Meteor. Soc.*, **88**, 513–526, https://doi.org/10.1175/bams-88-4-513.

Quiring, S., A. Schumacher, C. Labosier, and L. Zhu, 2011: Variations in mean annual tropical cyclone size in the Atlantic. *J. Geophys. Res.*, **116**, D09114, https://doi.org/10.1029/2010JD015011.

Song, J. J., and P. J. Klotzbach, 2016: Wind structure discrepancies between two best track datasets for western North Pacific tropical cyclones. *Mon. Wea. Rev.*, **144**, 4533–4551, https://doi.org/10.1175/MWR-D-16-0163.1.

Song, J. J., Y. H. Duan, and P. J. Klotzbach, 2020: Revisiting the relationship between tropical cyclone size and intensity over the western North Pacific. *Geophys. Res. Lett.*, **47**, e2020GL088217, https://doi.org/10.1029/2020GL088217.

Sun, Y., and Coauthors, 2017: Impact of ocean warming on tropical cyclone size and its destructiveness. *Sci. Rep.*, **7**, 8154, https://doi.org/10.1038/s41598-017-08533-6.

Wang, Y. Q., 2009: How do outer spiral rainbands affect tropical cyclone structure and intensity?. *J. Atmos. Sci.*, **66**, 1250–1273, https://doi.org/10.1175/2008JAS2737.1.

Weatherford, C. L., and W. M. Gray, 1988: Typhoon structure as revealed by aircraft reconnaissance. Part II: Structural variability. *Mon. Wea. Rev.*, **116**, 1044–1056, https://doi.

org/10.1175/1520-0493(1988)116<1044:TSARBA>2.0.CO;2.

Whitehead, J. C., 2003: One million dollars per mile? The opportunity costs of hurricane evacuation. *Ocean Coast. Manage.*, **46**, 1069–1083, https://doi.org/10.1016/j.ocecoaman.2003.11.001.

Willoughby, H. E., J. A. Clos, and M. G. Shoreibah, 1982: Concentric eye walls, secondary wind maxima, and the evolution of the hurricane vortex. *J. Atmos. Sci.*, **39**, 395–411, https://doi.org/10.1175/1520-0469(1982)039<0395:CEWSWM>2.0.CO;2.

Wu, L., and X. Lei, 2014: Preliminary research on the relationships between the inner core size and outer size of tropical cyclones and their intensity. *J. Trop. Meteor.*, **20**, 308–313, https://doi.org/10.16555/j.1006-8775.2014.04.002.

Ying, Y., and Q. H. Zhang, 2012: A modeling study on tropical cyclone structural changes in response to ambient moisture variations. *J. Meteor. Soc. Japan*, **90**, 755–770, https://doi.org/10.2151/jmsj.2012-512.

Yuan, J., D. Wang, C. Liu, and G. Wen, 2016: Validation of microwave-infrared, Tropical Rainfall Measuring Mission Microwave Imager and Advanced Microwave Scanning Radiometer–Earth observing system and WindSat-derived sea surface temperatures in coastal waters of the northern South China Sea. *Aquat. Ecosyst. Health Manage.*, **19**, 260–269, https://doi.org/10.1080/14634988.2016.1210444.

Yuan, J. N., D. X. Wang, Q. L. Wan, and C. Liu, 2007: A 28-year climatological analysis of size parameters for Northwestern Pacific tropical cyclones. *Adv. Atmos. Sci.*, **24**, 24–34, https://doi.org/10.1007/s00376-007-0024-y.

Yuan, J. N., C. Z. Zhang, G. H. Wen, M. Zhou, and Y. Zhu, 2024: Simulation of the effects of SST changes induced by tropical cyclones on the intensity of tropical cyclone Bilis (0604). *J. Trop. Meteor.*, **30**, 351–360, https://doi.org/10.3724/j.1006-8775.2024.031.

Zhang, K. L., and K. T. F. Chan, 2023: An ERA5 global climatology of tropical cyclone size asymmetry. *Int. J. Climatol.*, **43**, 950–963, https://doi.org/10.1002/joc.7846.

Citation: Yuan, J. N., G. H. Wen, M. S. Zhou, Y. Zhu, and Y. Zhu, 2026: The Rapid Shrinkage in Tropical Cyclone Sizes over the Western North Pacific. *J. Trop. Meteor.*, **32**, 229–238, https://doi.org/10.3724/j.1006-8775.2026.002.